47th AIAA Aerospace Sciences Meeting Including The New Horizons Forum and Aerospace Exposition
5 - 8 January 2009, Orlando, Florida

AIAA 2009-1461

A Surface Parameterization Method for Airfoil Optimization and High Lift 2D Geometries Utilizing the CST Methodology

Kevin A. Lane* and David D. Marshall†
California Polytechnic State University, San Luis Obispo, CA, 93407-0352

For aerodynamic modeling and optimization, it is desirable to limit the number of design variables to reduce model complexity and the requirements of the applied optimization scheme. The Class/Shape Transformation (CST) surface parameterization method presented by Kulfan has proven to be particularly useful for this while maintaining a wide range of applications. These include everything from smooth airfoils to 3D axi-symmetric bodies and wings. However, the CST method is confined to smooth geometries. This limits the CST method in applications incorporating discontinuous surfaces such as high lift aerodynamics with circulation control (CC) slots and flaps. The trailing edge slot on a circulation control wing (CCW) airfoil is not well modeled by the CST method. A parameterization of a CCW airfoil will result in the trailing edge slot being smoothed over. Therefore, a modified CST method must be utilized. For the case of parameterizing a known CCW airfoil, this is accomplished by detecting drastic changes in curvature and beginning a new parameterization in a "multi-surface parameterization" method. For creating a new CCW airfoil, this is achieved by modifying the 2D CST equations to incorporate a slot thickness term that also includes the horizontal location. These two methods can then be extended into 3D to model a circulation control wing (CCW) or even a blended wing body (BWB) aircraft incorporating CCW. The multi-surface parameterization modification can also be used to model other complex geometries to further enhance the robust nature of the CST method, thus creating a valuable design tool.

Nomenclature

α	=	angle of attack
ψ	=	non-dimensional streamwise location
η	=	non-dimensional semi-span location
ζ	=	non-dimensional vertical location
Δ	=	spacing
A	=	2D curvature coefficient array
b	=	wingspan
B	=	3D curvature coefficient matrix
c	=	chord length
C	=	class function
C_d	=	2D drag coefficient
C_l	=	2D lift coefficient
D	=	CST 2D geometry matrix
i	=	index of streamwise binomial coefficient
j	=	index of spanwise binomial coefficient
K	=	binomial coefficient
N	=	order of Bernstein polynomial
$N1$	=	first exponent in class function
$N2$	=	second exponent in class function
Nx	=	order of streamwise binomial coefficient
Ny	=	order of spanwise binomial coefficient

* Graduate Student, Aerospace Engineering Department, Student Member
† Associate Professor, Aerospace Engineering Department, Senior Member

Copyright © 2009 by David D. Marshall. Published by the American Institute of Aeronautics and Astronautics, Inc., with permission.

S	component shape function
t	arc length
x	streamwise location
y	spanwise location
z	vertical location

Subscripts

L	lower surface
LE	leading edge
U	upper surface
x	streamwise location
y	spanwise location

I. Introduction

The CST surface parameterization method is very powerful in its simplicity and ease of use. It is unique in that it can model a wide array of smooth geometries with a small number of equations and parameters. It is very similar to Bezier curves in that the CST equations are the Bezier curve equations with an added class function term. The class function classifies a shape into a particular category, which forms the base that all other shapes in that class are derived from. It can represent many aerodynamic shapes including a Sears-Haack body, biconvex airfoil, elliptic airfoil, wedge airfoil, and a round nose/pointed aft end airfoil resembling a NACA airfoil, as well as several others. These can be revolved to create an axi-symmetric body or can be altered with the shape function to obtain a new shape. The shape function determines the specific shape of the geometry within its class as specified by the class function. Other parameterization methods that have been used to model airfoils include Bezier curves, B-Splines, and NURBS. B-Splines and NURBS can have problems with oscillations when performing curve fits. CST does not have this problem. It results in smooth curves. CST can also fit a curve to a given airfoil with fewer coefficients than Bezier curves. This is because with a properly selected class function, the CST curve somewhat resembles the airfoil in question before any coefficients have been set.

II. Overview of CST Methodology

A) CST Airfoils

Any smooth airfoil can be represented by the general 2D CST equations. The only things that differentiate one airfoil from another in the CST method are two arrays of coefficients that are built into the defining equations. These coefficients control the curvature of the upper and lower surfaces of the airfoil. This gives a set of design variables which allows for aerodynamic optimization. This method of parameterization captures the entire design space of smooth airfoils and is therefore useful for any application requiring a smooth airfoil. The upper and lower surface defining equations are as follows:

$$\zeta_U(\psi) = C_{N2}^{N1}(\psi)\cdot S_U(\psi) + \psi\cdot\Delta\zeta_U$$
$$\zeta_L(\psi) = C_{N2}^{N1}(\psi)\cdot S_L(\psi) + \psi\cdot\Delta\zeta_L \tag{1}$$

where

$$\psi = x/c \quad \text{and} \quad \zeta = z/c$$

The last terms define the upper and lower trailing edge thicknesses. Equation uses the general class function to define the basic profile and the shape function to create the specific shape within that geometry class. The general class function is defined as:

$$C_{N2}^{N1}(\psi) = \psi^{N1}\cdot(\ \ -\psi)^{N2} \tag{2}$$

For a general NACA type symmetric airfoil with a round nose and pointed aft end, N is 0.5 and N2 is 1.0 in the class function. This classifies the final shape as being within the "airfoil" geometry class, which forms the basis of CST airfoil representation. This means that all other airfoils represented by the CST method are derived from the class function airfoil. This is due to the fact that if the shape function equals one everywhere, the resulting airfoil is

equivalent to that given by the class function. Therefore, to represent an airfoil with the CST method, N1 and N2 can be replaced with 0.5 and 1.0 respectively. Equation 1 then becomes:

$$\begin{aligned}\zeta_U(\psi) &= C_{1.0}^{0.5}(\psi)\cdot S_U(\psi)+\psi\cdot\Delta\zeta_U \\ \zeta_L(\psi) &= C_{1.0}^{0.5}(\psi)\cdot S_L(\psi)+\psi\cdot\Delta\zeta_L\end{aligned} \tag{3}$$

Many other classes exist, but the 2D analysis will be limited to airfoils for now. Figure displays the NACA type airfoil as represented by the class function.

Figure 1: General airfoil defined with class function.

The shape function defines the specific shape within the airfoil class. The overall shape functions for the upper and lower surfaces are as follows:

$$\begin{aligned}S_U(\psi) &= \sum_{i=0}^{N_U} A_U(i)\cdot S(\psi,i) \\ S_L(\psi) &= \sum_{i=0}^{N_L} A_L(i)\cdot S(\psi,i)\end{aligned} \tag{4}$$

where S is the component shape function and is represented by a Bernstein polynomial. N is the order of the Bernstein polynomial used for either the upper or lower surface. This is also equal to one less than the number of curvature coefficients used. The component shape function is scaled by the curvature coefficients which determines the specific airfoil shape. The component shape function is given as the following:

$$S(\psi,i) = K_i^N\cdot\psi^i\cdot(\ -\psi)^{N-i} \tag{5}$$

where K is the binomial coefficient, which is directly related to the order of the Bernstein polynomials used. The binomial coefficient is defined as:

$$K_i^n = \frac{n!}{i!(n-i)!} \tag{6}$$

Equations 2-6 can be combined to form the complete equations to represent the upper and lower surfaces of CST airfoils.

$$\begin{aligned}\zeta_U(\psi) &= \psi^{0.5}\cdot(\ -\psi)^{1.0}\sum_{i=0}^{N_U}\left[A_U(i)\cdot\frac{N_U!}{i!(N_U-i)!}\cdot\psi^i\cdot(\ -\psi)^{N_U-i}\right]+\psi\cdot\Delta\zeta_U \\ \zeta_L(\psi) &= \psi^{0.5}\cdot(\ -\psi)^{1.0}\sum_{i=0}^{N_L}\left[A_L(i)\cdot\frac{N_L!}{i!(N_L-i)!}\cdot\psi^i\cdot(\ -\psi)^{N_L-i}\right]+\psi\cdot\Delta\zeta_L\end{aligned} \tag{7}$$

Equation 7 fully describes any smooth airfoil given the correct curvature coefficients. These coefficients can be optimized to represent a known airfoil, which can also serve as a starting point for an airfoil geometry optimization. Having an airfoil parameterized by the CST method gives an equation for the upper and lower surfaces. This allows points to be added at desired locations to refine areas such as the leading edge of an airfoil that has high curvature. Figure 2 shows some examples of parameterized airfoils to display the power of the CST surface parameterization method. The circles show the exact airfoil coordinates and the lines correspond to the CST airfoil surface calculated using optimized curvature coefficients. The coefficients were calculated by minimizing the root mean squared error

between the exact coordinates and the CST coordinates. This was performed using the MATLAB[2] optimizer **`fminunc`**.

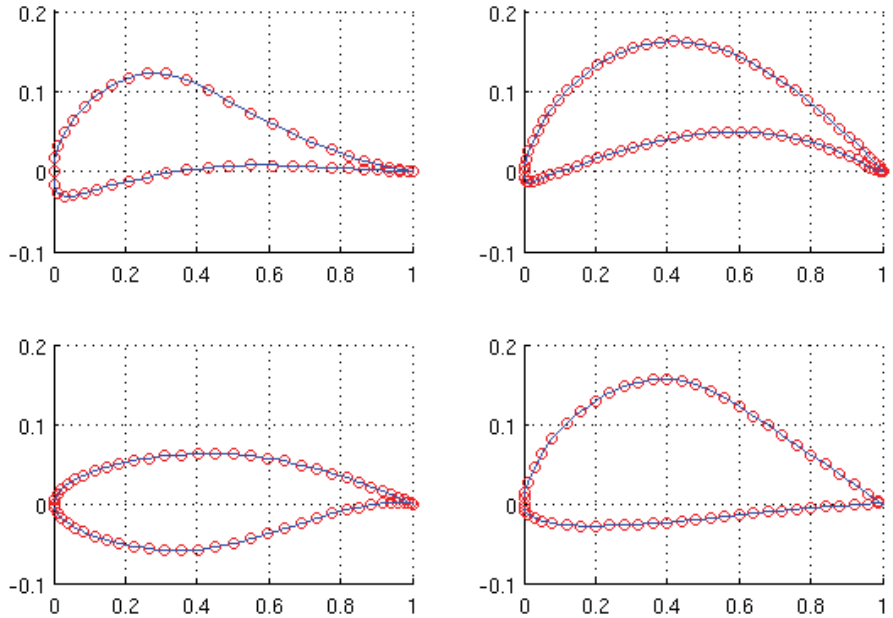

Figure 2: Airfoils parameterized using curvature coefficient optimization.

B) CST Wings

The 2D process for airfoils is easily extended to wings as a simple extrusion of parameterized airfoils. This greatly increases the number of design variables for an optimization scheme. However, it is no less powerful. By controlling the distribution of airfoils, any smooth wing can be represented. Also, such characteristics as sweep, taper, geometric twist, and aerodynamic twist can be included. The definition of a 3D surface follows a similar structure to that of a 2D surface. The upper and lower surface defining equations for a 3D CST surface are as follows.

$$\zeta_U(\psi,\eta) = C_{N2}^{N1}(\psi)\cdot\sum_{i=0}^{Nx_U}\sum_{j=0}^{Ny_U}\{[B_U(i,j)\cdot S_y(\eta,j)]\cdot S_x(\psi,i)\}+\psi\cdot\{-\tan[\alpha_{TWIST}(\eta)]\}$$

$$\zeta_L(\psi,\eta) = C_{N2}^{N1}(\psi)\cdot\sum_{i=0}^{Nx_L}\sum_{j=0}^{Ny_L}\{[B_L(i,j)\cdot S_y(\eta,j)]\cdot S_x(\psi,i)\}+\psi\cdot\{-\tan[\alpha_{TWIST}(\eta)]\} \tag{8}$$

where

$$\psi = \frac{x-x_{LE}(\eta)}{c(\eta)} \quad \text{and} \quad \eta = \frac{2\mathrm{y}}{b}$$

and where the unit streamwise and unit spanwise shape functions are:

$$S_x(\psi,i) = K_i^{Nx}\cdot\psi^i\cdot(\ -\psi)^{Nx-i}$$
$$S_y(\eta,j) = K_j^{Ny}\cdot\eta^j\cdot(\ -\eta)^{Ny-j} \tag{9}$$

Just as with a CST airfoil, a CST wing is based on an extension of an airfoil defined with the class function. Therefore, Eq. 8 can be rewritten to represent a wing by using 0.5 for N1 and 1.0 for N2.

$$\zeta_U(\psi,\eta) = C_{1.0}^{0.5}(\psi)\cdot\sum_{i=0}^{Nx_U}\sum_{j=0}^{Ny_U}\{[B_U(i,j)\cdot S_y(\eta,j)]\cdot S_x(\psi,i)\}+\psi\cdot\{-\tan[\alpha_{TWIST}(\eta)]\}$$
$$\zeta_L(\psi,\eta) = C_{1.0}^{0.5}(\psi)\cdot\sum_{i=0}^{Nx_L}\sum_{j=0}^{Ny_L}\{[B_L(i,j)\cdot S_y(\eta,j)]\cdot S_x(\psi,i)\}+\psi\cdot\{-\tan[\alpha_{TWIST}(\eta)]\} \quad (10)$$

The last terms in Eq. 10 allow for geometric twist by simply entering the desired angle of twist. Also, by controlling the leading edge location and chord length distributions, wing sweep and taper can easily be achieved. This is displayed in Figure 3.

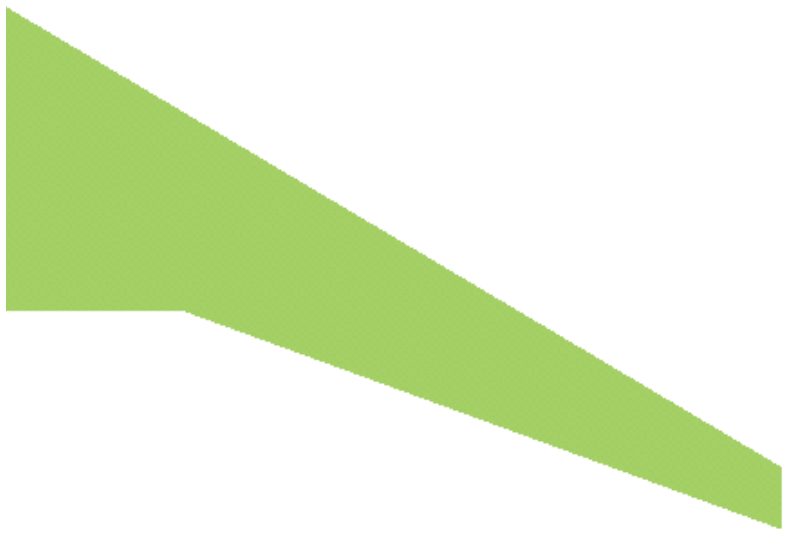

Figure 3: CST generate wing with sweep and taper.

The B_U and B_L terms are essentially matrices of the curvature coefficients discussed for airfoils. This permits easy implementation of aerodynamic twist. By controlling the distribution of curvature coefficients in the spanwise direction, the cross-section of the wing can be varied. The wing from Figure 3 is rotated and cross-sections are shown along the span in Figure 4 to better display this. Aerodynamic twist can be seen by the change in the airfoil throughout the cross-sections shown. The airfoil warps slightly between each cross-section to provide a smooth transition from the root airfoil to the tip airfoil. Aerodynamic twist is shown by the difference in the tip and root airfoils. The root airfoil is symmetric while the tip airfoil is cambered.

Figure 4: Spanwise slices of wing generated via CST demonstrating aerodynamic twist.

See Kulfan for a more thorough discussion of the application of the CST method to smooth airfoils and wings, as well as other aircraft components such as nacelles.

III. Improvements to the CST Method

Starting from the basic CST methodology, important improvements have been made to improve the speed of solving for the unknown coefficients, via pseudo-inverses, and the accuracy of the representation, via modifying the class function terms. In addition, a parameterized variation of the CST method was explored in order to improve the robustness of the representation of vertical edges.

A) Analytical Solution for Curvature Coefficients

An analytical solution for the curvature coefficients was recently discovered and implemented for this work. The general CST equations for two-dimensional curves given above can be represented as:

$$\vec{\zeta} = \quad \cdot \vec{A} + \vec{\psi} \cdot \Delta\zeta$$

$$= \begin{matrix} C_{N2}^{N1}\ \psi(0)] \cdot K_0^N \cdot \psi(0)^{\,0} \cdot [\ -\psi(0)]^{N-0} & C_{N2}^{N1}\ \psi(0)] \cdot K^N \cdot \psi(0)\ \cdot [\ -\psi(0)]^{N-} & \cdots \\ C_{N2}^{N1}\ \psi(\ \ )] \cdot K_0^N \cdot \psi(\ \ )^{\,0} \cdot [\ -\psi(\ \ )]^{N-0} & C_{N2}^{N1}\ \psi(\ \ )] \cdot K^N \cdot \psi(\ \ )\ \cdot [\ -\psi(\ \ )]^{N-} & \\ \vdots & & \ddots \end{matrix} \tag{1}$$

where $\vec{A}$ is the Bernstein polynomial coefficients and is the only unknown term. Since D is only a square matrix if the order of the Bernstein polynomial equals the number of points used to represent the airfoil, the pseudo inverse, $^{+}$, is used to solve for the curvature coefficients. This minimizes the least squared difference between the given $\vec{\zeta}$ values and the calculated ones.

$$\vec{A} = \quad ^{+}(\vec{\zeta} - \vec{\psi}\,\Delta\zeta) \tag{12}$$

This analytical solution was compared to the optimizer solution to determine its merits. It was discovered that the analytical solution either matched or bettered the optimizer solution throughout the entire range of orders tested and had a significantly shorter runtime. Therefore, it became the method of choice over the optimizer method.

B) N1 and N2 Optimization Study

It was desirable to study the effects of varying N and N2 to see if there existed better choices for N and N2 than the given values of 0.5 and 1.0 respectively. N and N2 were optimized using the MATLAB optimizer **`fminunc`** and the analytical solution mentioned in the previous section. Figure 5 displays a comparison of the RMS error and the

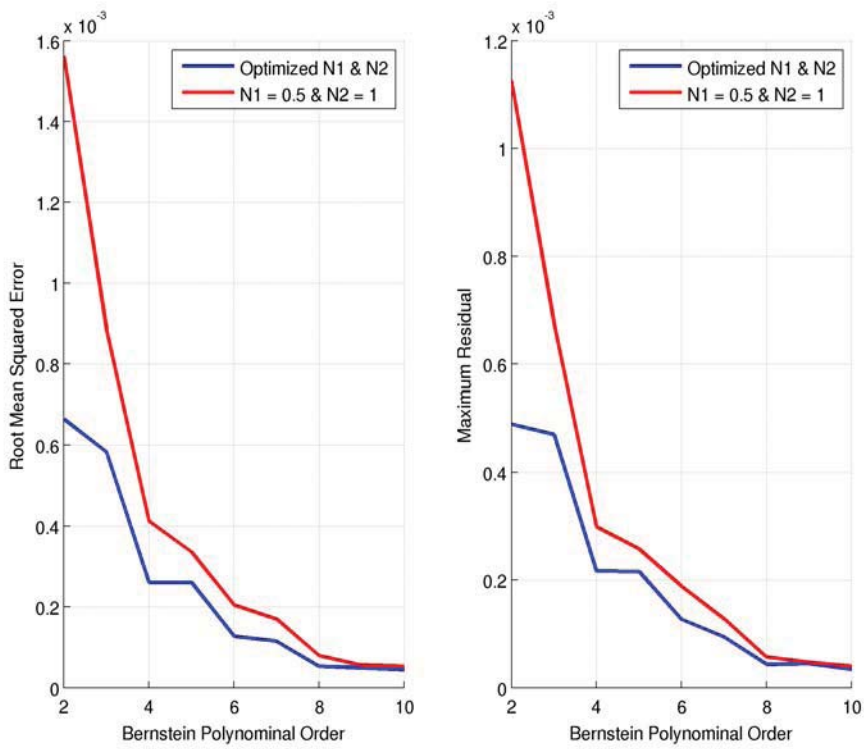

Figure 5: Error for optimized and fixed N1 and N2 coefficients in the class function.

maximum residual for the fit of an RAE2822 airfoil over a range of Bernstein polynomial orders. It clearly shows that the optimized N1 and N2 coefficients yield a better fit than using N and N2 values of 0.5 and 1.0 respectively. While optimization results in more accurate solutions, given the scale of the y-axes, an N1 of 0.5 and an N2 of 1.0 is often acceptable for achieving a good fit without having to perform an optimization. However, using optimized N and N2 values would prove to be useful when highly accurate representations are required.

One thing to note is that while 0.5 and 1.0 are not optimal values for N and N2, they are close. This is why they were selected as the general coefficients to represent the airfoil class. The optimized values of N1 and N2 do not differ much from the given values of 0.5 and 1.0. Table displays the optimized values of N1 and N2 for each order tested for the same test case of the RAE2822 airfoil.

Table 1: Optimized values of the class function parameters for an RAE 2822 airfoil.

Order	N1	N2
2	0.4843	.0684
3	0.4703	.0330
4	0.4973	0.9262
5	0.4977	0.9277
6	0.4780	.0017
7	0.4829	.0281
8	0.4931	0.9614
9	0.4956	0.9752
0	0.4926	0.9946

C) Parameterized CST

It was desirable to develop a fully parameterized CST method where the ψ and ζ coordinates are calculated at a given arc length t along the curve as opposed to the current method of solving for an ζ coordinate at a given ψ value. This would permit parameterization of shapes with vertical segments, such as CCW airfoils. This was performed by creating a parameterized equation for the ψ values. A D_x matrix similar to the aforementioned D matrix can be constructed that is dependent upon arc length. This can be used to solve for the $\vec{A}_x$ coefficients that represent the given ψ values.

$$_x = \begin{matrix} K_0^N \cdot t(0)^{\,0} \cdot [\ \ -t(0)]^{N-0} & K^N \cdot t(0)\ \ \cdot [\ \ -t(0)]^{N-} \\ K_0^N \cdot t(\ \ )^{\,0} \cdot [\ \ -t(\ \ )]^{N-0} & K^N \cdot t(\ \ )\ \ \cdot [\ \ -t(\ \ )]^{N-} \end{matrix} \tag{13}$$

The $\vec{A}_x$ coefficients are determined as the product of the pseudo inverse of the D_x matrix and the known ψ values.

$$\vec{A}_x = \ _x^{\,+} \cdot \vec{\psi} \tag{14}$$

A similar D_y matrix is equivalent to the D matrix in Eq. where the ψ values correspond to the parameterized values above.

$$_y = \begin{matrix} C_{N2}^{N1}\ \psi(0)] \cdot K_0^N \cdot \psi(0)^{\,0} \cdot [\ \ -\psi(0)]^{N-0} & C_{N2}^{N1}\ \psi(0)] \cdot K^N \cdot \psi(0)\ \ \cdot [\ \ -\psi(0)]^{N-} \\ C_{N2}^{N1}\ \psi(\ \ )] \cdot K_0^N \cdot \psi(\ \ )^{\,0} \cdot [\ \ -\psi(\ \ )]^{N-0} & C_{N2}^{N1}\ \psi(\ \ )] \cdot K^N \cdot \psi(\ \ )\ \ \cdot [\ \ -\psi(\ \ )]^{N-} \end{matrix} \tag{15}$$

Similarly, the $\vec{A}_y$ coefficients are determined by using the pseudo inverse of the D_y matrix.

$$\vec{A}_y = {}_y^{+}(\vec{\zeta} - \vec{\psi}\,\Delta\zeta) \tag{16}$$

Therefore, the parameterized 2D CST equations become:

$$\begin{aligned} \psi(t) &= \sum_{i=0}^{N} A_x(i)\cdot K_i^N \cdot t^i \cdot (\quad -t)^{N-i} \\ \zeta(t) &= C_{N2}^{N1}\ \psi(t)]\cdot \sum_{i=0}^{N}\{A_y(i)\cdot K_i^N \cdot \psi(t)^i \cdot [\quad -\psi(t)]^{N-i}\} + \psi(t)\cdot\Delta\zeta \end{aligned} \tag{17}$$

This method introduces additional variables into the system. Two sets of curvature coefficients are required to represent a parameterized CST airfoil. However, it is a more general representation in that both coordinates are calculated at a specific distance along the curve as opposed to the original method where a ζ value is calculated using a given ψ value.

IV. Airfoil Optimization

As previously explained, the CST method gives equations for the upper and lower surfaces of an airfoil in terms of the curvature coefficients. These coefficients can be used as design variables in an aerodynamic optimization scheme. Such a scheme is currently being developed to maximize the lift to drag ratio (L/D) of a supercritical airfoil for use on a next generation commercial airliner. The optimization scheme uses the MATLAB function **`fmincon`** as the optimizer. This function was selected over **`fminunc`** so that constraints could be placed on the airfoil geometry.

Computational fluid dynamics (CFD) was selected for the solution method because the optimization is performed in the transonic regime where many other solution methods are not valid. This complicates the process greatly. Since CFD is to be used by an optimizer, both the meshing and solution processes must be automated. Therefore, the meshing process must be robust enough to handle any airfoil selected by the optimizer. However, the meshing process will still be sensitive to the given airfoil geometry. If the airfoil selected by the optimizer is too unlike the airfoil used to develop the meshing automation, the meshing process is prone to errors. Therefore, constraints are used to force the optimizer to select airfoils that somewhat resemble the initial airfoil. Constraints implemented to ensure an airfoil successfully passes the meshing stage include limits on maximum thickness and minimum thickness. An additional constraint was placed so that the upper surface does not cross the lower surface.

The objective function of the optimization scheme uses ICEM CFD[3] for meshing and FLUENT[4] for solving. Both these steps are fully automated and have been implemented in the objective function. The optimizer is currently being tested for a cruise condition of Mach 0.8 at an altitude of 35,000 feet. To ensure that a constant C_l is maintained, the objective function estimates the current airfoil's lift curve by fitting a line to C_l values taken from CFD solutions at different angles of attack. This is used to obtain the angle of attack that should produce the desired C_l. This angle of attack is used for the final CFD solution of the objective function from which L/D is taken and read by the optimizer.

The initial airfoil selected for the optimization scheme was the RAE 2822 transonic airfoil previously used in the class function coefficient optimization study. A C_l of 0.322 was selected to correspond to the C_l at cruise of the airfoil used by a next generation commercial airliner currently being studied at Cal Poly. Table 2 Displays a comparison between the performance of the initial and optimized airfoils. The C_l values differ somewhat and displays some error in the selection of angle of attack. However, the C_d of the optimized airfoil is dramatically lower than that of the initial airfoil. The C_d value drops from 273 drag counts to 140, which is a reduction of 133 drag counts or about 49%. This also causes the L/D to increase from 12.05 to 22.78, which is an increase of about 89%.

Table 2: Performance comparison of initial and optimized airfoils.

	Initial Airfoil	**Optimized Airfoil**
C_l	0.329	0.318
C_d	0.0273	0.0140
L/D	12.05	22.78
α (degrees)	0.96	1.5

Figure 6 displays the L/D throughout the optimization process. It shows that the optimizer makes two significant improvements in L/D and otherwise changes very little. This phenomena is interesting and is under further investigation.

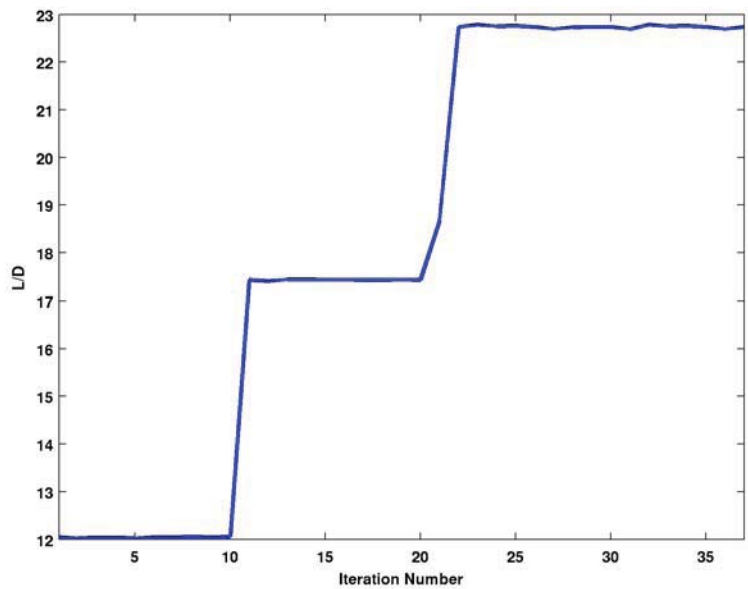

Figure 6: Variation of L/D throughout optimization

V.Figure 7 displays contours of Mach number over the initial and optimized airfoils. The initial airfoil is displayed on the left while the optimized airfoil is shown on the right. The maximum Mach number in the flow over the initial airfoil is much higher than that of the optimized airfoil. This is because the upper surface of the optimized airfoil is much flatter than that of the initial airfoil, which causes the flow to accelerate less over the upper surface of the optimized airfoil. This is the cause of the dramatic drag reduction. The lowest point of the lower surface of the optimized airfoil is forward from that of the initial airfoil. This allows for lower speed flow and therefore higher pressure.

Figure 8 displays contours of static pressure over the initial and optimized airfoils. The static pressure is much more negative over the upper surface of the initial airfoil than that of the optimized airfoil. This is to be expected given the higher velocity flow over the initial airfoil. Also, the suction peak is moved forward from that of the initial airfoil.

Figure 9 displays contours of entropy over the initial and optimized airfoils. A weak shock exists near the trailing edge of the initial airfoil as evident by the light contour extending above the upper surface near the trailing edge. No shock exists on the optimized airfoil. There is no entropy contour extending above the upper surface as is the case with the initial airfoil.

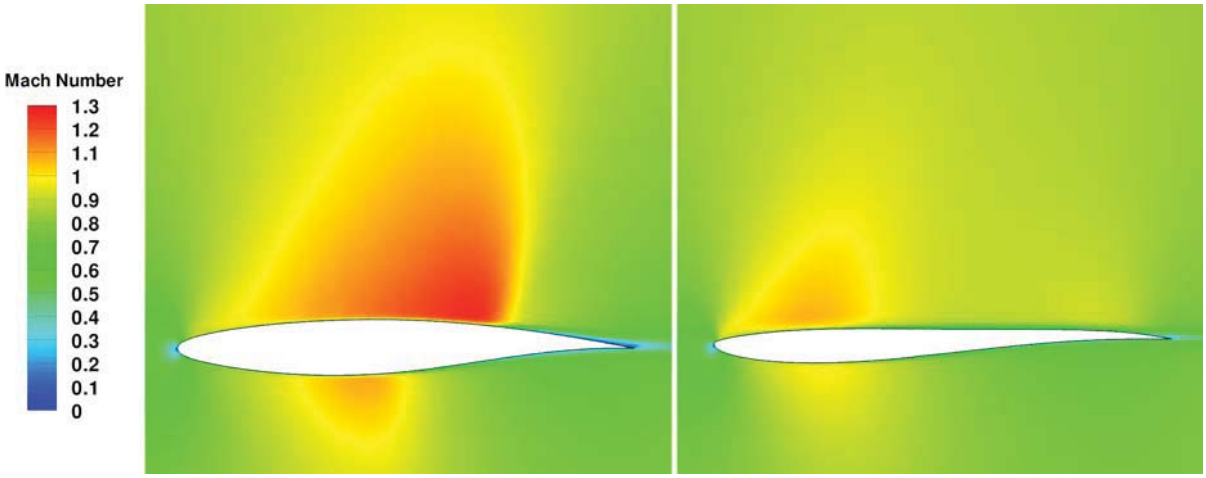

Figure 7: Contours of Mach number for the initial airfoil (left) and the optimized airfoil (right).

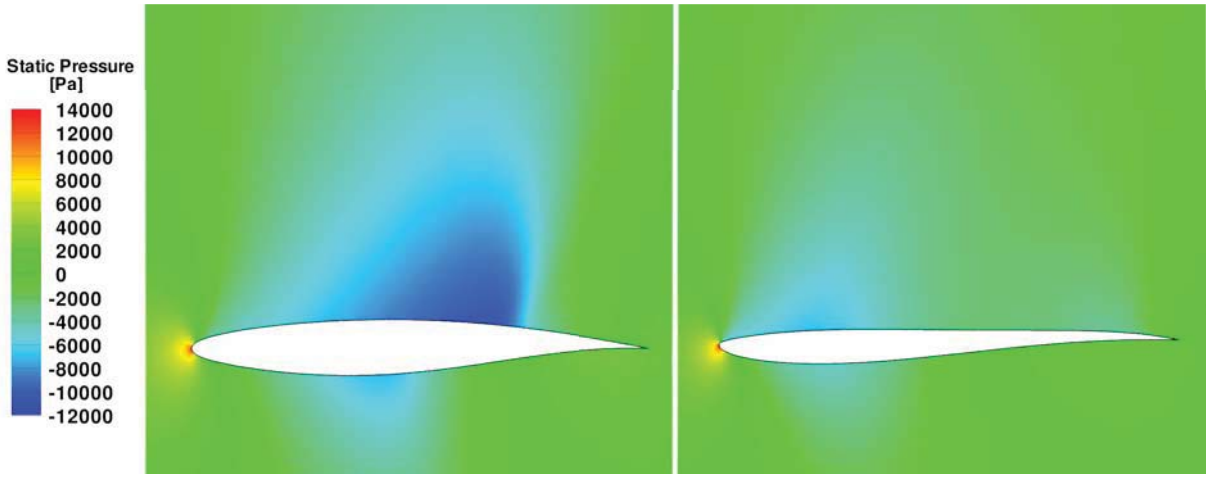

Figure 8: Contours of static pressure for the initial airfoil (left) and the optimized airfoil (right).

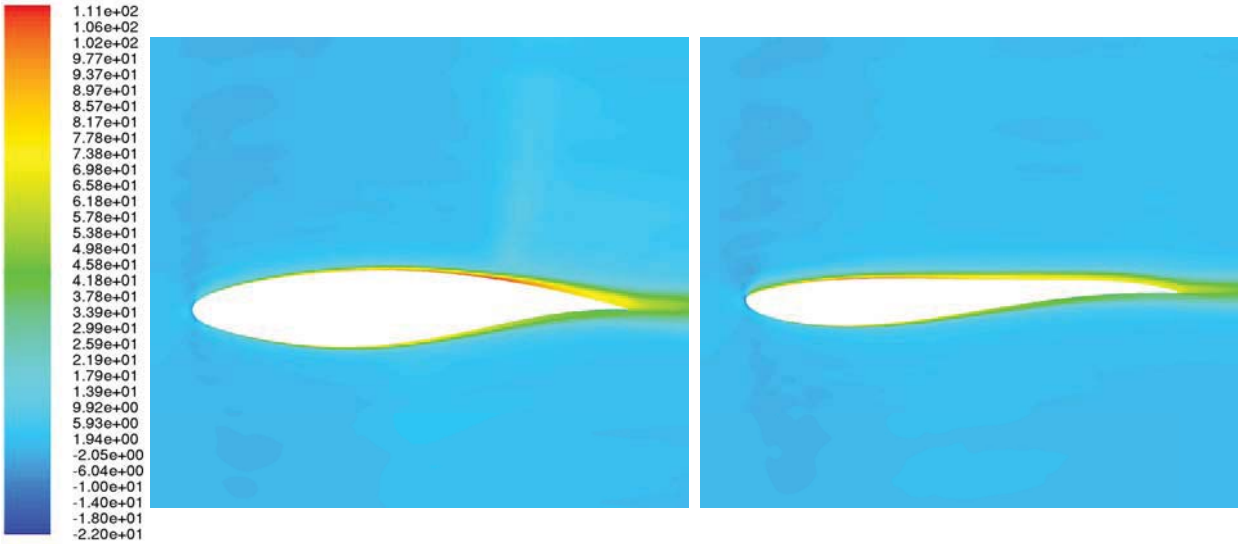

Figure 9: Contours of entropy for the initial airfoil (left) and the optimized airfoil (right).

Figure 10 displays contours of Mach number throughout the optimization. Iterations 11 and 21 are shown along with the initial airfoil and the optimized airfoil (iteration 23). Iterations and 21 were selected in the middle of the optimization because these are the iterations that showed the biggest change besides iteration 22. This was not shown because it very closely resembles the optimized airfoil. Iteration has a has much more rapid acceleration around the upper leading edge but with a lower maximum Mach number at the suction peak. The upper surface shock for this iteration is not nearly as severe and results in an increase in L/D to 17.43. Iteration 21 shows two shocks on the upper surface, one near the mid-chord and one near the trailing edge, with the trailing edge shock formed because of the thicker trailing edge compared to iteration 11. However, they are both weaker than the shocks of the initial airfoil and iteration 11. The lower surface shows an increase in the amount of decelerated flow which yields a larger pressure force associated with that surface. This results in an increase of L/D to 18.68. After this point, the optimizer reached airfoils very close to the optimized airfoil. Figure 10 gives an indication of what the optimizer is doing. First, it finds a way to eliminate the shock on the upper surface by flattening the upper surface. This results in less acceleration over the upper surface. This is shown by the shocks getting weaker throughout the optimization. The optimizer then works on increasing the pressure on the lower surface.

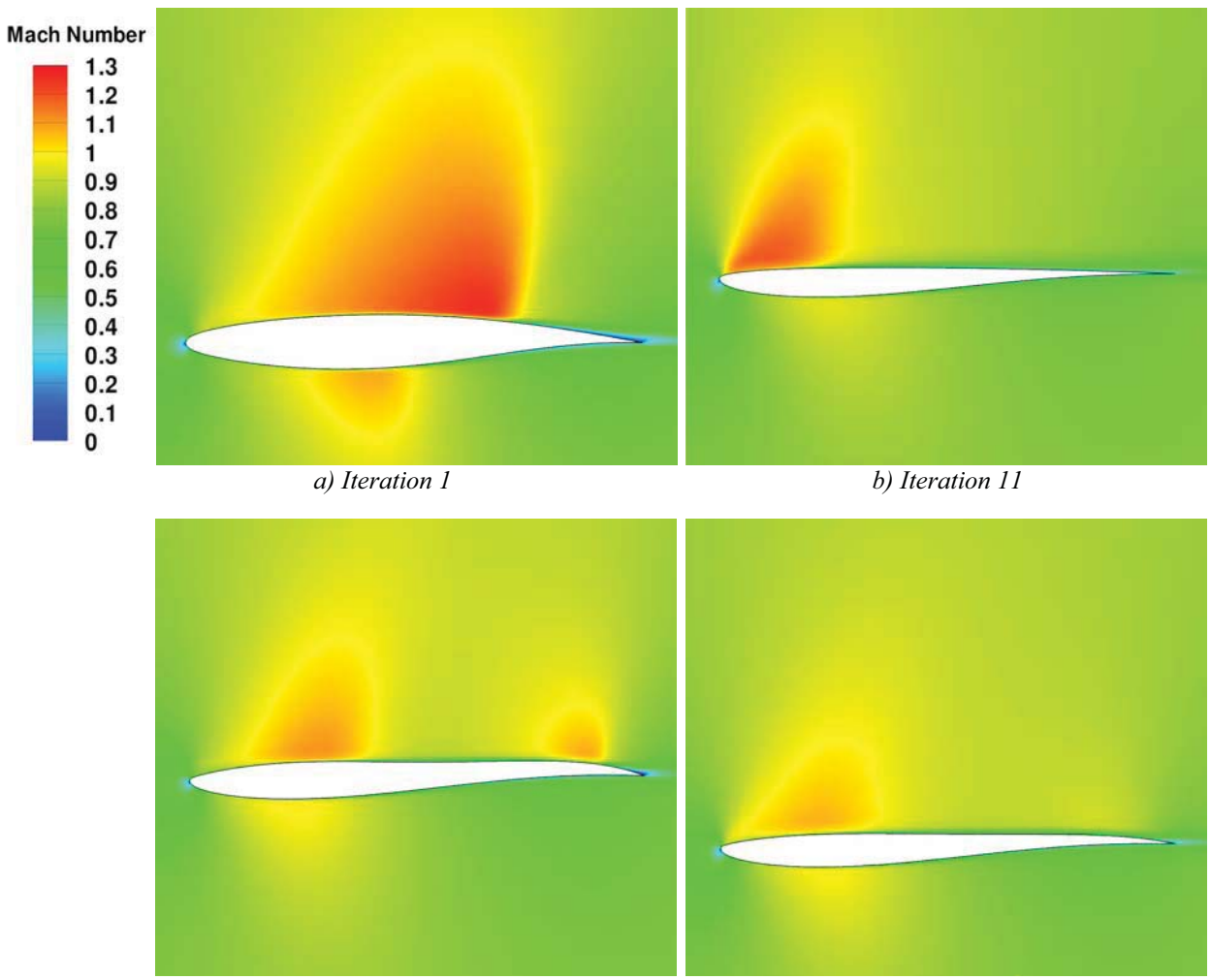

a) Iteration 1 *b) Iteration 11*

c) Iteration 21 *c) Iteration 23*

Figure 10: Contours of Mach number throughout the optimization.

VI. Application of CST to CCW Airfoils

Since the CST method, when applied to airfoils, only works for those that are smooth, modifications must be made if the method is to be used to parameterize more complex geometries, such as a CCW slot. The general CST method

smooths over the slot when parameterizing a circulation control airfoil, which is illustrated in Figure where the red circles signify the airfoil coordinates and the blue line represents the CST curve approximation.

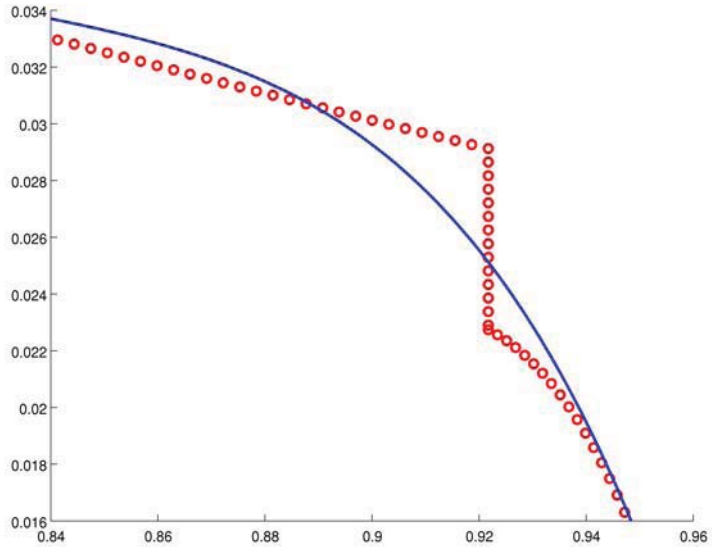

Figure 11: Unsplit CST representation of a CCW airfoil.

To account for this problem, the upper surface had to be split into three segments. This was performed by detecting the smoothness of the airfoil surface. The dot product of three consecutive points was taken and used to determine the angle between the vector from the first to the second point and the vector from the second to the third point. This was done along the entire airfoil surface and if the angle was determined to be too great, the surface was split at that location. This proved to yield a much better representation of the CCW airfoil in question. The multi-surface CST representation of the CCW airfoil is shown below in Figure 12.

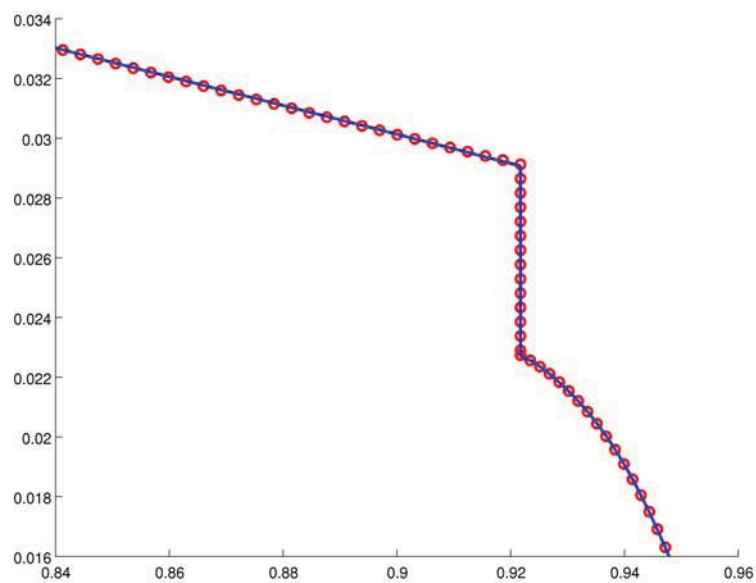

Figure 12: Multi-surface CST representation of a CCW airfoil.

It is clearly evident that the multi-surface CST method well represented the CCW airfoil by splitting the airfoil at the top and bottom of the slot. This allowed CST curves to be created to represent three smooth sections as opposed to one surface with drastic changes in curvature. This method allows a designer to focus on specific sections of an airfoil, which is a valuable attribute when designing such complex geometries.

VII. Future Work

The airfoil optimization scheme is still in development and has room for improvement. The C_l values of the initial and optimized airfoils showed some variation during the optimization process (as much as 3% of the target). This needs to be rectified through a more refined process of estimating each airfoil's lift curve. Also, the optimized airfoil was much thinner than the initial airfoil, which could produce structural problems. Therefore, an additional constraint will be placed on the airfoil area to create a structural constraint without performing any structural analysis.

A second CFD automation is being developed for CCW airfoils. Once completed, this can be used in a similar optimization scheme as the one previously discussed. Having a parameterized CCW airfoil gives several options for design variables in the optimization. The height of the CCW slot and the shape of the flap can be optimized in addition to the shape of the upper and lower surfaces.

As previously mentioned, a wing is simply an extrusion of airfoil cross-sections in the CST method. This allows a CCW airfoil parameterized with one of the methods mentioned in the previous section to be included on a CCW. This allows the CCW slot to be placed along any portion of the trailing edge of the wing, permitting another aspect of the wing to be optimized. The root of the wing can also be modified to more closely represent a fuselage, thus allowing a BWB aircraft to be parameterized with the CST method. Work in this area is ongoing.

VIII. Acknowledgements

This work was funded as part of a NASA Research Announcement award under Contract #NNL07AA55C with Craig Hange and Joe Posey as the technical monitors. The authors wish to thank Brenda Kulfan for her fruitful discussions about the CST method. The help of John Pham in this work on the FLUENT automation and post processing is greatly appreciated.

IX. References

Kulfan, B. M.,"A Universal Parametric Geometry Representation Method – 'CST'," *45th AIAA Aerospace Sciences Meeting and Exhibit*, January, 2007. AIAA 2007-0062.

[2]MATLAB, Software Package, Version 7.5.0.338 (R2007b). The Mathworks Inc., Natick, MA, 2007.

[3]ICEM CFD, Software Package, Version 11.0.1. Ansys Inc., Canonsburg, PA.

[4]FLUENT, Software Package, Version 6.3.26. Ansys Inc., Lebanon, NH.